# Supporting Information

**Fabricating scattering-fluorescent luminescent solar concentrator synchronously to achieve broad-spectrum solar energy utilization and light pollution inhibition**

*Chenkai Jin [ab], Chengqi Feng [a,*], Yuhua Chen[a], Ting Zhang [a], Huiwen He[b], Haining Na [ab,*] and Jin Zhu [a]*

[a] Key Laboratory of Bio-Based Polymeric Materials of Zhejiang Province, Ningbo Institute of Materials Technology and Engineering, Chinese Academy of Sciences, Ningbo, Zhejiang 315201, China

[b] School of Materials Science and Engineering, Zhejiang University of Technology, Hangzhou, Zhejiang 310014, China

**Corresponding Author: nahaining@nimte.ac.cn; fengchengqi@nimte.ac.cn;*

*Tel: +86-574-86689806; Fax: +86-574-86685186.*

## Experimental Section

### Materials

Citrate acid (AR grade, 99%), urea (AR grade, 99%), tris (hydroxymethyl) aminomethane hydrochloride (Tris-HCl) (AR grade, 99%), ethylene imine polymer (PEI, $M_w$ equals to 600, 1800 and 10000 respectively, AR grade, 99%), methyl methacrylate (AR grade, 99%) and 2,2'-azobis (2-methylpropionitrile) (AR grade, 99%) were obtained from Aladdin Co., Ltd. Microfibrillated cellulose (MFC) (water content of 98%, with diameter of 0.1-1.0 μm and length over 20 μm) was purchased from Guilin Qihong Technology Co., Ltd. All the other reactants were in chemical grade and used without further purification.

### Methods

### Synthesis of MFC/CQDs composite

Citric acid (2 g) and urea (4 g) were added to deionized water (45 mL), fully dissolved and added to a 100 mL hydrothermal reactor lined with polytetrafluoroethylene. The reaction was carried out at 160 °C for 3 h. After cooling, the reaction solution was filtered with a 0.2 μm filter membrane. The filtrate was

concentrated by rotary evaporation and then transferred into a dialysis bag with an intercepted capability of molecular weight at 1000 Da. After dialysis for 48h, a purified solution with carbon quantum dots (CQDs) is obtained. Different series of CQDs were obtained by controlling reaction time and reaction temperature.

Tris-HCl (1 g) was added to a solution of CQDs (10 mL) and stirred with a magnet bar for 15 min at 400 rpm. PEI (0.3 g) was added and kept on stirring for 12 h at room temperature. Then, MFC (5 g) was added to the solution by vigorously stirring for 12 h. After loading CQDs on MFC, the whole mixture was centrifuged at 8000 rpm for 10 min to pick out the solid product. The obtained MFC/CQDs composite was washed with deionized water under ultrasonic wave agitation at 10 min for 5 cycles. The type and amount of PEI to induce the formation of MFC/CQDs composite was also researched in the experiment.

**Synthesis of LSCs**

Ethanol was first utilized to displace the water in the MFC/CQDs composite completely. A certain amount of ethanol-infiltrated MFC/CQDs composite was added to MMA (10 mL) and stirred until uniformly dispersed. AIBN (0.2wt%) was added to the mixture and stirred for 20 min. After that, the temperature was raised to 80 °C for pre-polymerization for 15 min. Then, the pre-polymerized mixture was poured into a mold composed of double pieces of glass with a rubber sealing ring. The air bubble was expelled. The inlet of the glass mold was clamped with steel clips. The whole glass mold was put in an oven at 60 °C for 12 h. After polymerization, it was picked out and cut into the size of 2 × 2 × 0.2 $cm^3$. After simply polishing the edges, a luminescent solar concentrator (LSC) was finally obtained.

**Construction of PV-LSCs device**

One edge of the two series of LSCs was fixed on the silicon photovoltaic cell ($J_{SC}$=39.08 mA/$cm^2$, $V_{OC}$=0.54 V, *PCE*=14.79%, which were obtained in the photoelectric performance test of LSCs; and the effective area of the battery is 0.4 $cm^2$ except for occlusion) with UV-curable adhesive, respectively. The uncovered part of the photovoltaic cell was covered with a mirror paste and then covered with a label paper (to avoid interference of incident light) to make a PV-LSC device. Furthermore,

two edges of the LSCs are also tried to fix on the photovoltaic cell, to create a series circuit in the device. So that, adequate voltage can be provided to light the diode.

**Characterization**

The morphology of materials was characterized by using a scanning electron microscope (SEM, S4800, Hitachi, Japan), a transmission electron microscope (TEM, JEM2100, JEOL, Japan), and an atomic force microscope (AFM, VeecoMultiMode/NanoScope IIIa, Bruker, USA), respectively. The Elemental composition and chemical state of CQDs were characterized with an X-ray photoelectron spectroscopy (XPS, AXIS Ultra DLD, Kratos Analytical, U.K.). High-resolution X-ray diffraction measurements were conducted by use of an X-ray Powder diffractometer (XRD, D8 ADVANCE DAVINCI, Bruker, Germany). The wavelength of the X-ray was 1.5406 Å (Cu $K_\alpha$ radiation, 40 kV and 100 mA) in a 2θ range between 5° and 90°, and the scanning rate was 6 °/min. The infrared absorption spectra of CQDs were recorded on Fourier transform infrared spectroscopy (FTIR, Nicolet 6700, Thermo Fisher Scientific, USA), and the number of scans was set to 32. The infrared absorption spectra of the MFC/CQDs composite were recorded on a microscopic infrared spectrometer (Cary660+620, Agilent, USA), and the number of scans was set to 32. The UV-vis absorption, transmittance, and reflectivity of materials were measured on a UV/Vis/NIR spectrophotometer (Lambda 950, Perkin-Elmer, US) at the wavelength between 250 nm and 800 nm. The structure of CQDs was characterized by a Raman spectroscopy (Renishaw PLC, Wotton-under-edger, U.K.) with a laser wavelength of 532 nm. The fluorescence spectrum, photoluminescence quantum yield (PLQY), and the fluorescence lifetime were measured by a fluorescence spectrometer (FL3-111, HORIBA, France). The excitation slit and emission slit were both 1.5 nm. The PLQY was measured by spectrometers with a built-in integrating sphere. The Zeta potential of the MFC/CQDs composite at neutral pH value was measured by Laser Doppler Micro-electrophoresis (Zetasizer Nano ZS, Malvern, UK) equipped with platinum electrodes at room temperature. Thermogravimetric analysis (TGA) of the MFC/CQDs composite was performed by a thermogravimetric analyzer (TG209F1, Netzsch, Germany) from 25

°C to 800 °C in a nitrogen atmosphere at the scanning rate of 10 °C/min. The crystalline morphology of LSCs was investigated by polarized optical microscopy (POM, BX51, OLYMPUS, Japan). The microscopic fluorescence images of LSCs were obtained from laser scanning confocal microscopy (LSCM, TCS SP5, Leica, Germany). Light J-V curves were measured by using a Keithley 2400 source meter under a light intensity of 100 mW/cm$^2$ (AM 1.5G) from the Class AAA solar simulator (EnliTech, China). The $\eta_{opt}$ of LSCs was obtained from a multimeter (UT533, UNI-T, China) under a light intensity of 100 mW/cm$^2$ (AM 1.5G). In the darkroom scattering experiment, LSCs were placed in a smaller hole to observe the light spot in the homemade darkroom at room temperature.

**Calculations**

The external optical efficiency ($\eta_{opt}$) and *PCE* of the LSCs were further measured by coupling the power meter at the edge of the LSCs. The $\eta_{opt}$ refers to the ratio of the power coming out of the slab edge of the LSCs ($P_{out}$) to the power coming in ($P_{in}$) through the top surface. The $\eta_{opt}$ can be simply defined as follows,[1]

$$\eta_{opt} = \frac{P_{out}}{P_{in}} = \frac{I_{LSC} \times A_{edge}}{I_{SC} \times A_{top}} = \frac{I_{LSC}}{I_{SC} * G} \quad (1)$$

where $I_{LSC}$ is the short circuit current from the PV cell attached to the LSC, and $I_{SC}$ is the short circuit current measured from the same solar cell directly with the same light source. The geometric gain $G$ is a ratio of the LSC slab's top surface area ($A_{top}$) to the edge surface area ($A_{edge}$).[1]

$$G = \frac{A_{top}}{A_{edge}} \quad (2)$$

Another important parameter used to define the performance of a PV-LSC device is the overall power conversion efficiency (*PCE*) defined as,[2]

$$PCE = \frac{J_{sc} \times V_{oc} \times FF}{P_{in}} \quad (3)$$

where $J_{sc}$ is the short circuit current density (The area used 0.4 cm$^2$, only measured one edge of LSC), $V_{oc}$ is the open-circuit voltage, and *FF* is the fill factor that can be obtained from the photocurrent density-voltage (J-V) curves. $P_{in}$ (AM 1.5G, 100

mW/cm$^2$) is the irradiation intensity.

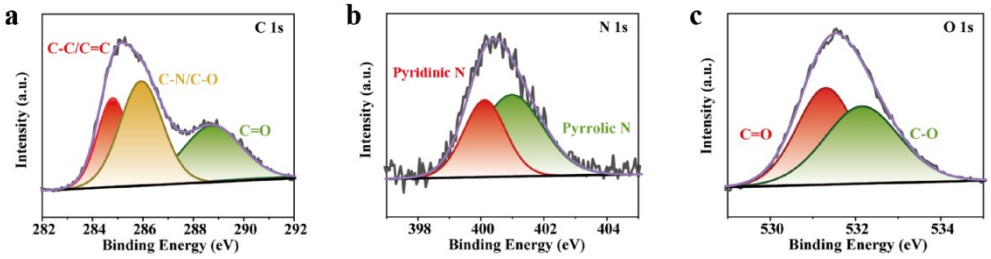


**Fig. S1** High-resolution XPS fitting results for C 1s (a), N 1s (b), and O 1s (c) of CQDs.

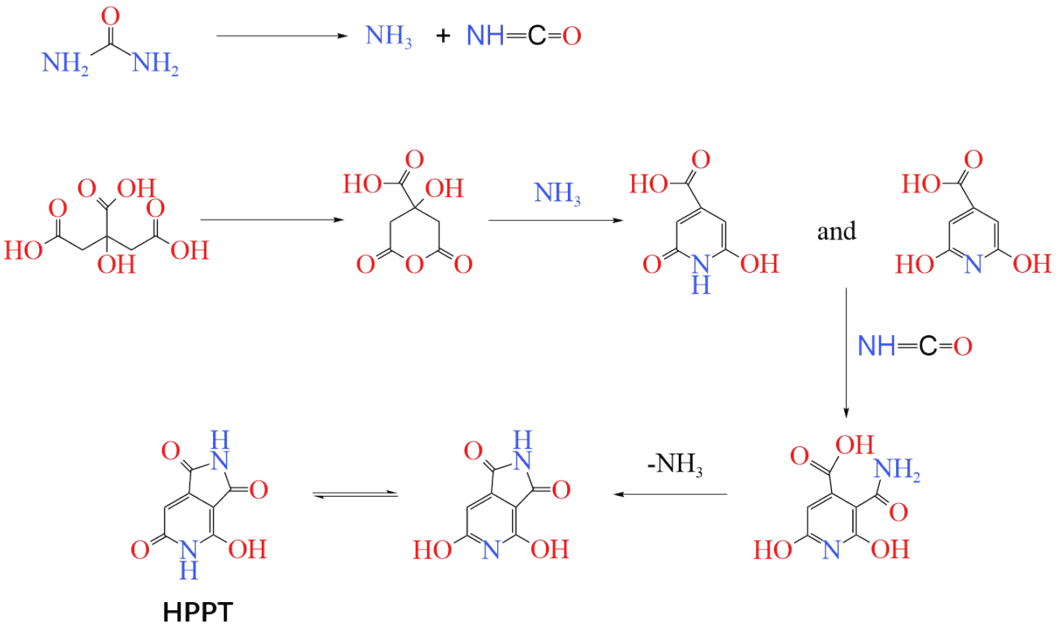


**Fig. S2** Formation of HPPT through the reaction of urea and citrate acid. [3-4]

The synthesis of CQDs by N doping strategy starts from the formation of 4-hydroxy-1*H*-pyrrolo[3,4-*c*]pyridine-1,3,6(2*H*,5*H*)-trione (HPPT). After that, HPPT and its derivatives react with unreacted monomers through keto-enol tautomerism, intramolecular dehydration, and amidation reaction to form a fluorescent carbon layer and then gradually stacks into CQDs through π-π interaction and hydrogen bond interaction. This is also consistent with the actual microstructure of the obtained CQDs.

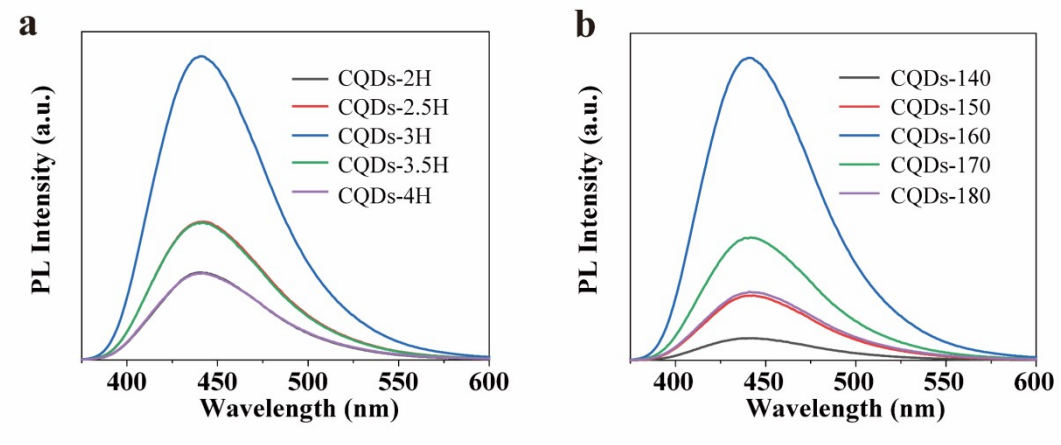


**Fig. S3** PL spectra of CQDs obtained with different reaction times (a) and reaction temperatures (b).

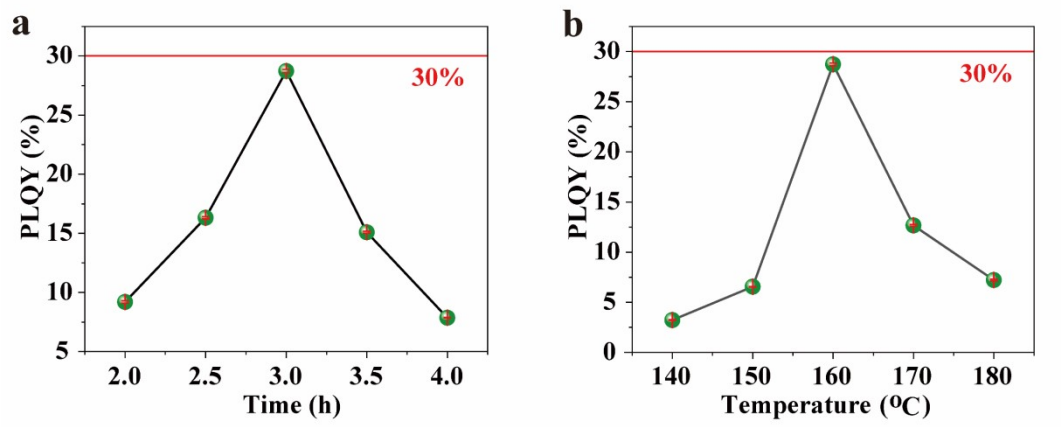


**Fig. S4** PLQY of CQDs obtained with different reaction times (a) and reaction temperatures (b).

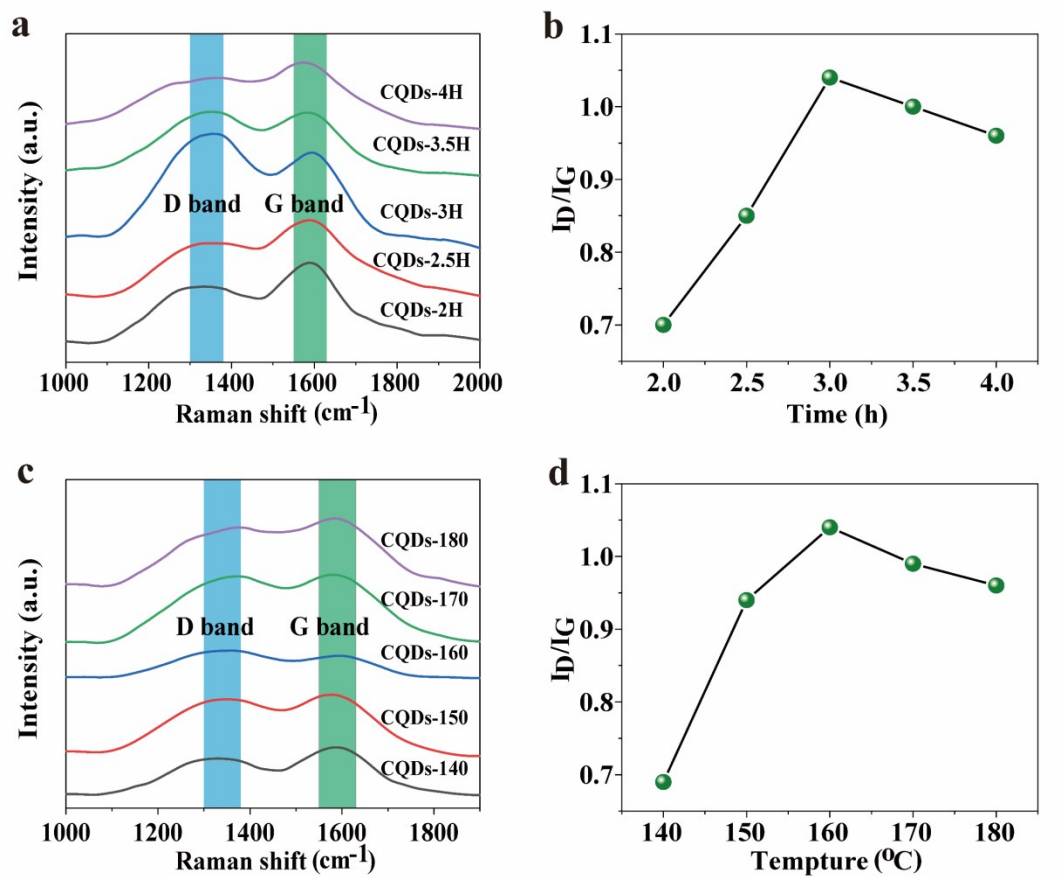


**Fig. S5** Raman analysis of CQDs obtained with different reaction times (a-b) and reaction temperatures (c-d).

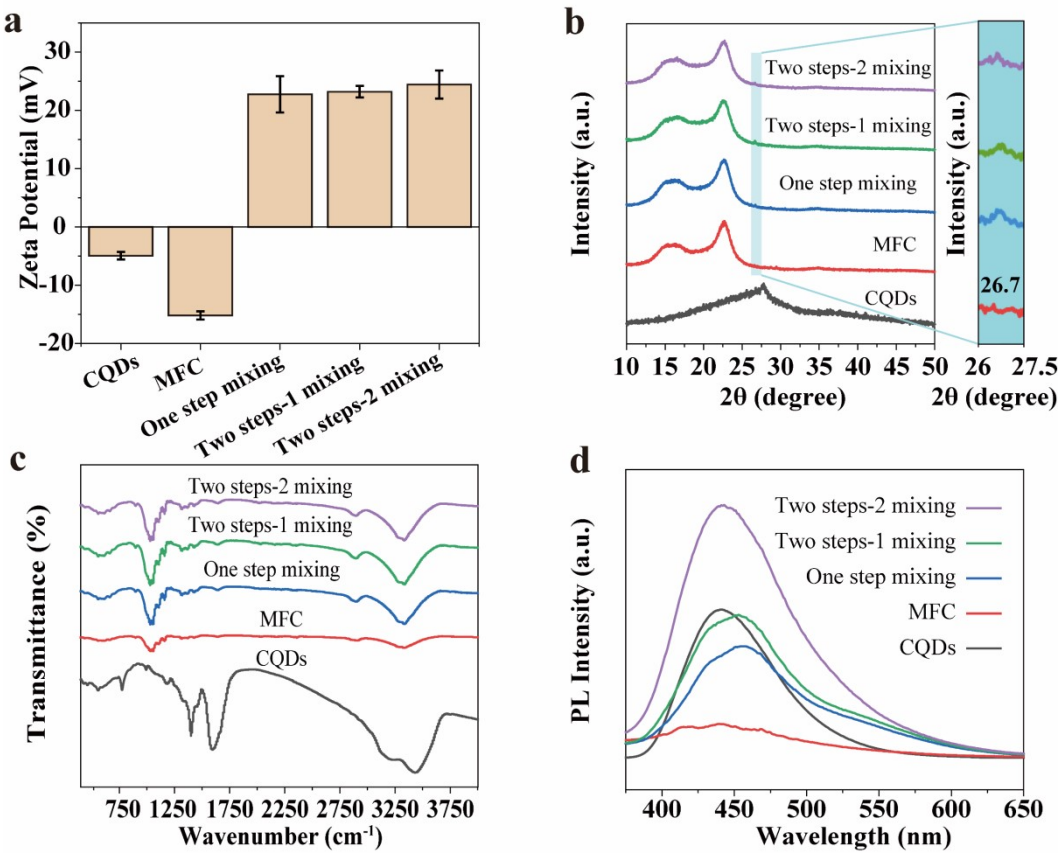


**Fig. S6** Zeta potential (a), XRD patterns (b), FTIR spectra (c) and PL spectra (d) of CQDs, MFC, and their composites prepared by a different process including One-step mixing (namely mixing MFC, CQDs, and $PEI_{10000}$ in one pot directly), Two-step-1 mixing (firstly mixing MFC with $PEI_{10000}$ and then continue to mix with CODs) and Two-step-2 (firstly mixing CQDs with $PEI_{10000}$ and then continues to mix with MFC).

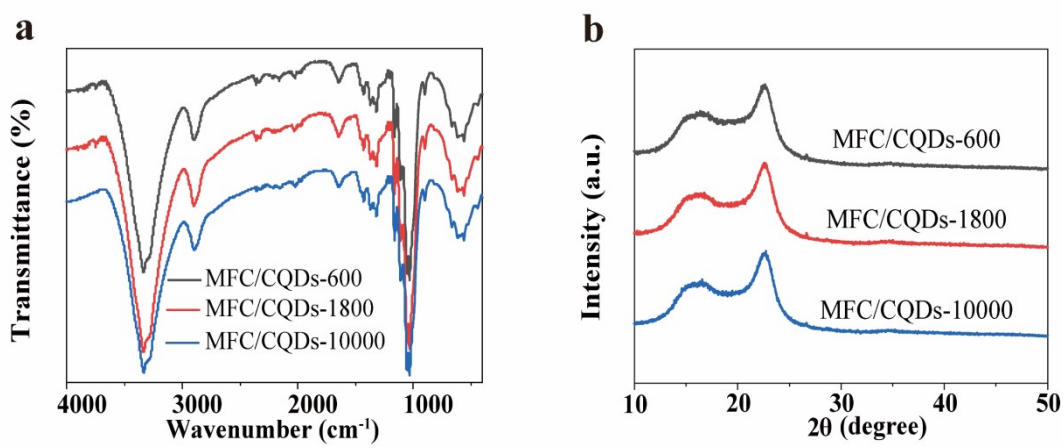


**Fig. S7** FTIR spectra (a) and XRD patterns (b) of MFC/CQDs composites prepared with PEI of different molecular weights.

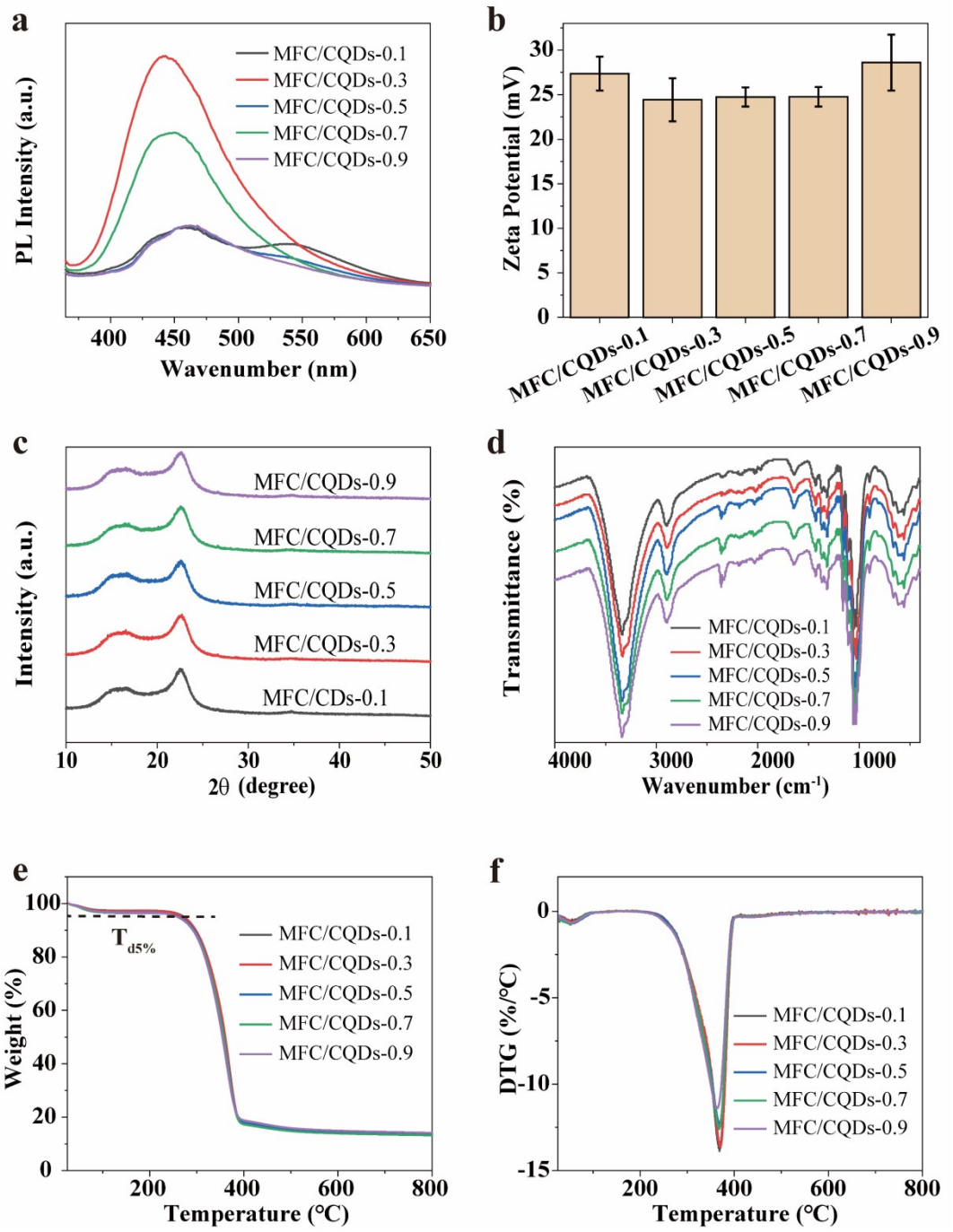


**Fig. S8** PL spectra (a), Zeta potential (b), XRD pattern (c), FTIR spectrum (d), TGA curves (e) and DTG curves (f) of MFC/CQDs composites prepared with $PEI_{10000}$ at different amounts.

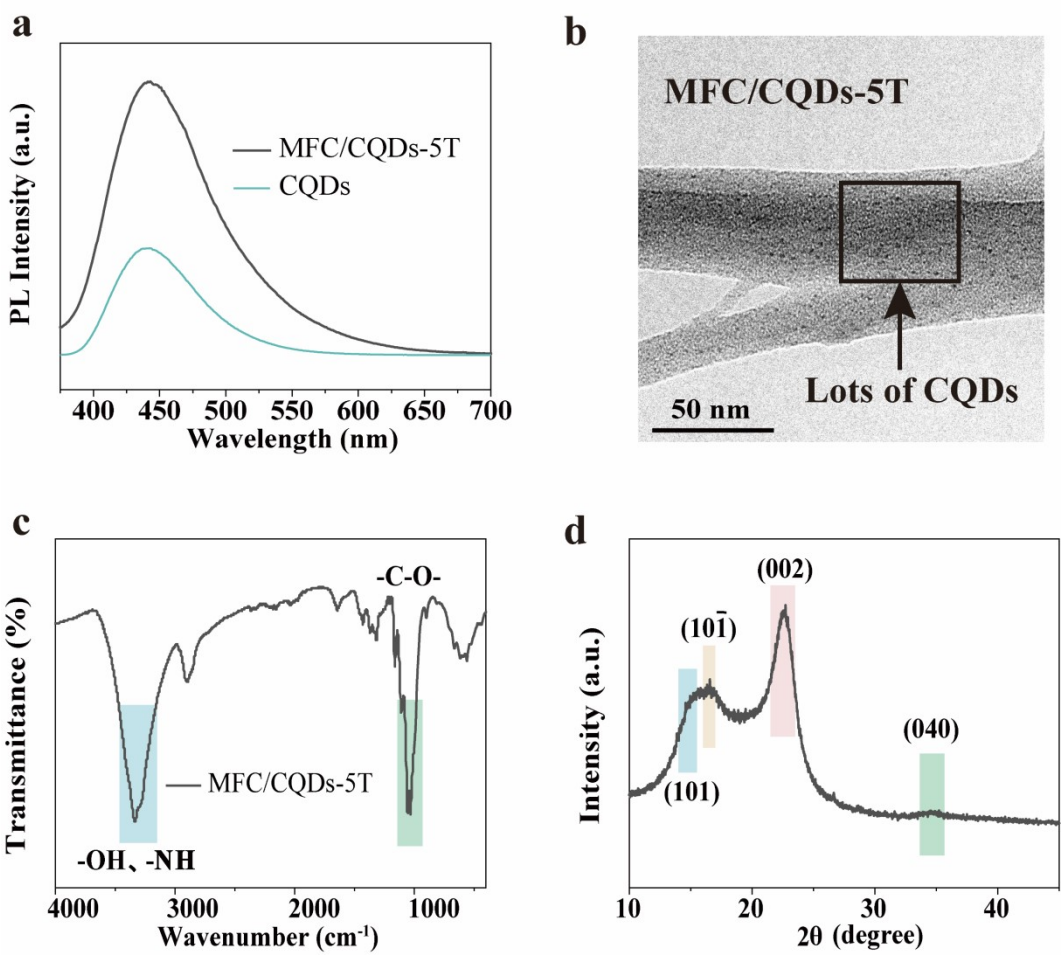


**Fig. S9** PL spectra (a), TEM micrograph (b), FTIR spectrum (c), and XRD pattern (d) of MFC/CQDs composites before and after being washed with deionized water for 5 times.


**Fig. S10** Dispersed state of MMA with MFC/CQDs or MFC under different mixing modes.

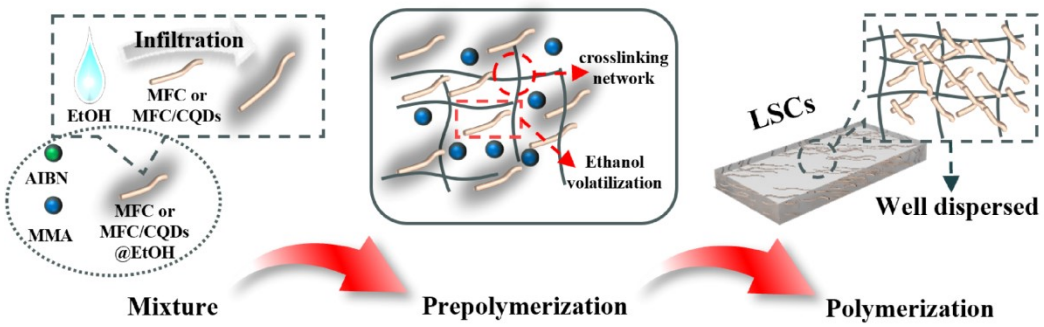


**Fig. S11** Dispersion mechanism of MFC/CQDs in PMMA during in-situ radical bulk polymerization.

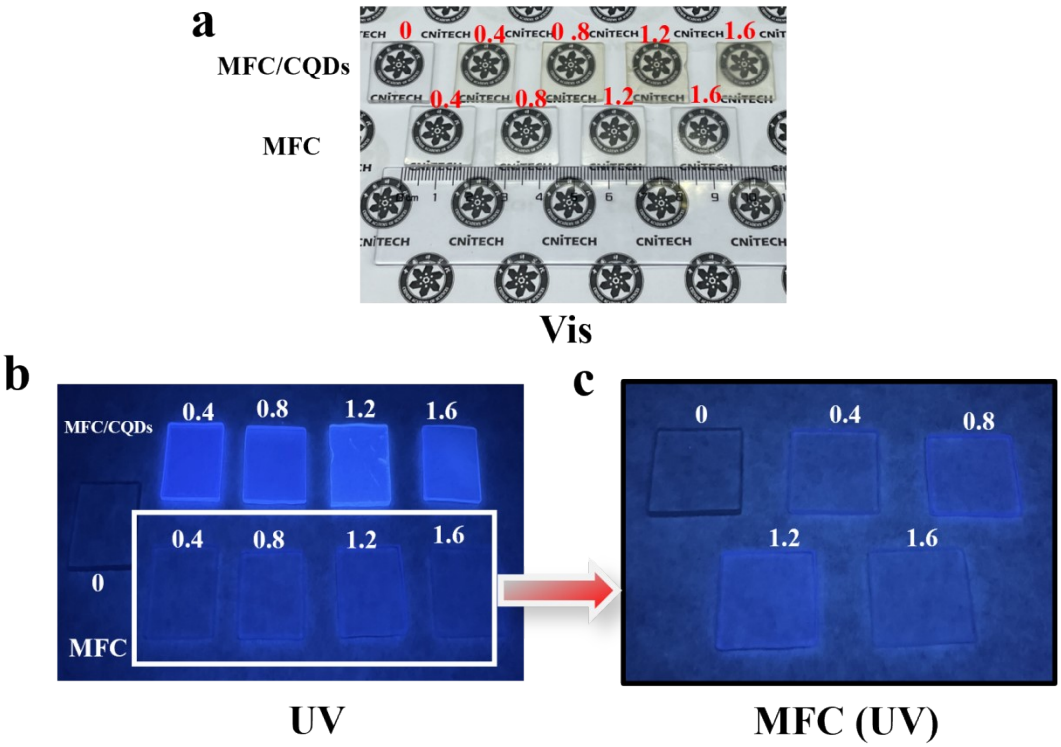


**Fig. S12** Digital photos of LSCs with different mass fractions of MFC and MFC/CQDs composite under sunlight (a) and their photos under ultraviolet light (b-c).

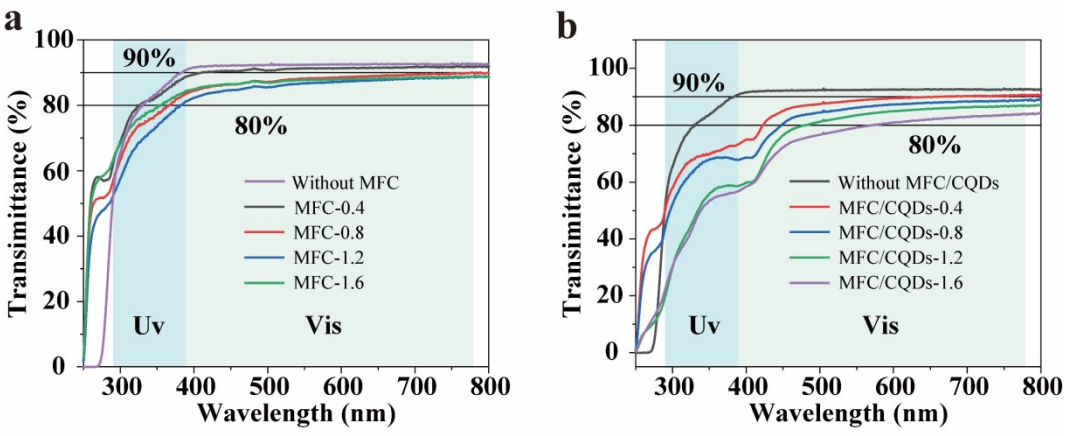


**Fig. S13** UV-vis transmittance of LSCs with different mass fractions of MFC (a) and MFC/CQDs composite (b).

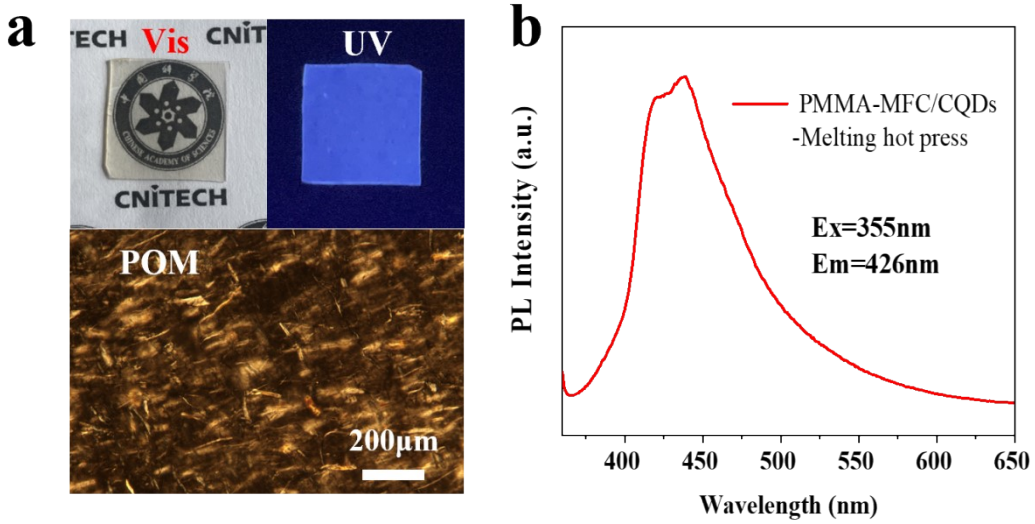


**Fig. S14** Digital photos under sunlight and ultraviolet light, POM micrograph (a), and PL spectrum of PMMA-MFC/CQDs LSC after secondary hot-press molding (b).

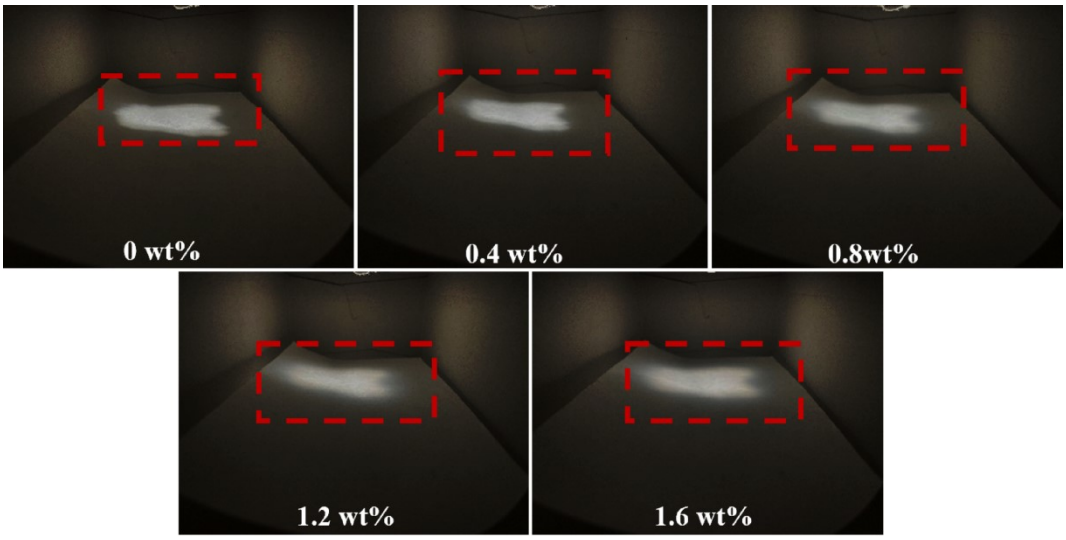


**Fig. S15** Digital scattering photos of LSCs of PMMA-MFC with different mass fractions of MFC under natural light.

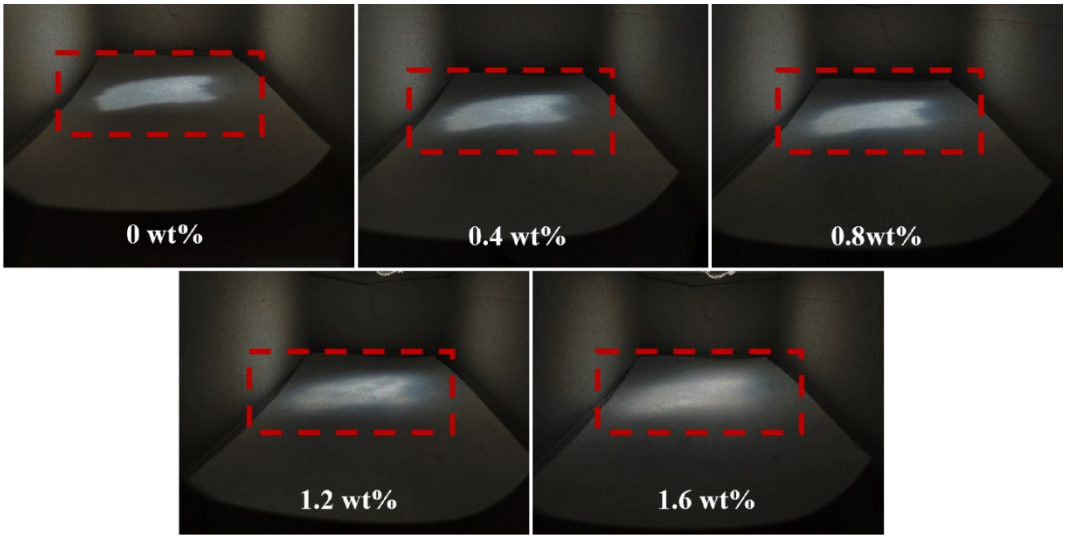


**Fig. S16** Digital scattering photos of LSCs of PMMA-MFC/CQDs with different mass fractions of MFC/CQDs composite under natural light.

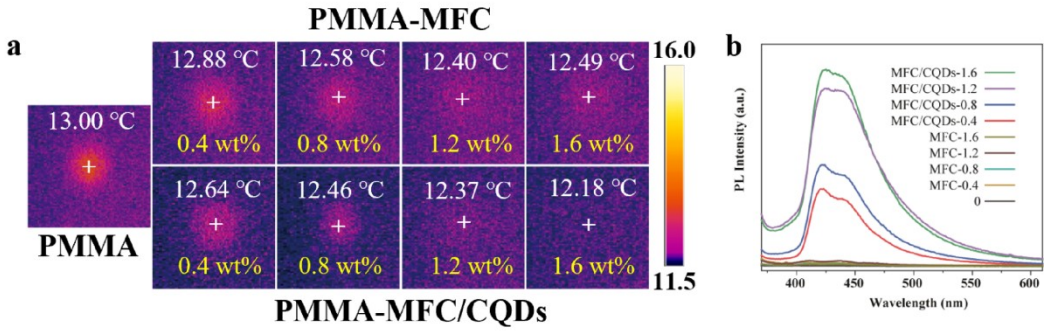


**Fig. S17** Scattering light spot infrared thermal imaging (a) and PL spectra (b) of the LSCs with different amounts of MFC and MFC/CQDs.

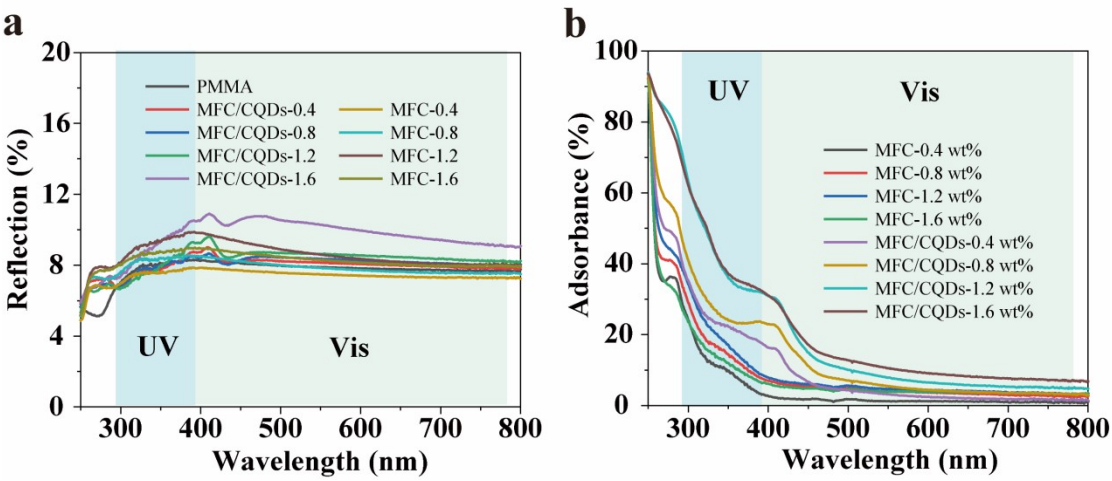


**Fig. S18** UV-vis reflection (a) and absorbance (b) of LSCs with different MFC and MFC/CQDs amounts. Each data point is calculated (The formula is A = 100%-T-R).

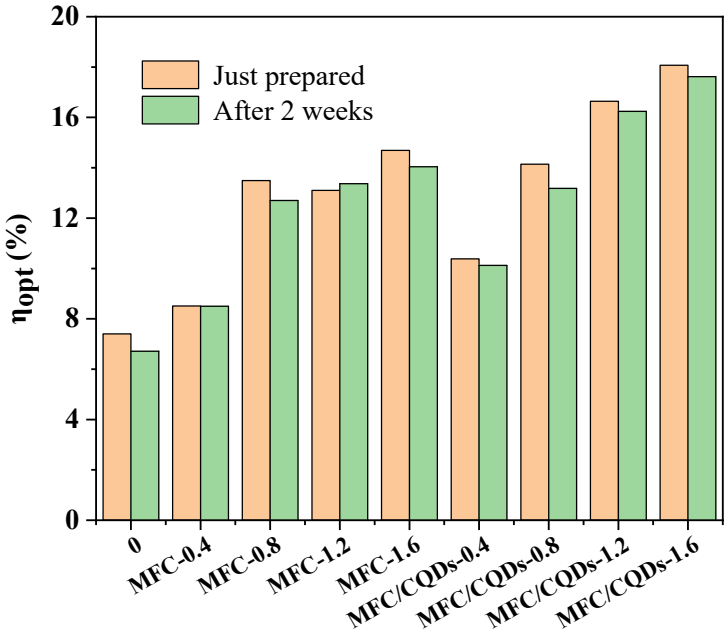


**Fig. S19** $\eta_{opt}$ of PV-LSC device with different amounts of MFC and MFC/CQDs just prepared and after located under natural conditions for 2 weeks.

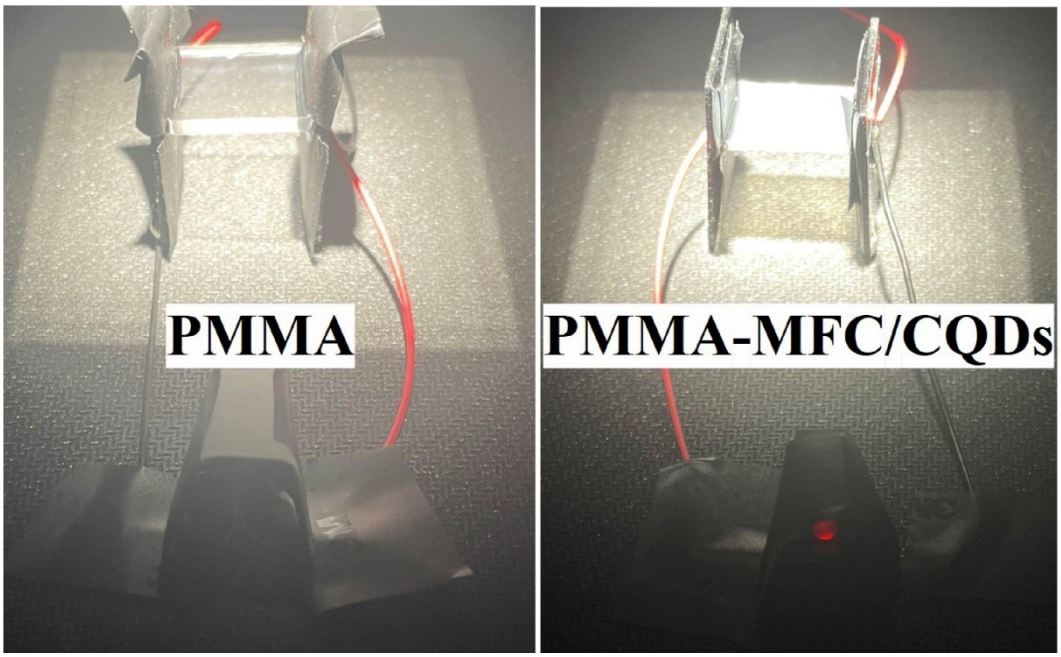


**Fig. S20** Digital photos of PV-LSC devices prepared by S-L LSC and pure PMMA to light LED lamp.

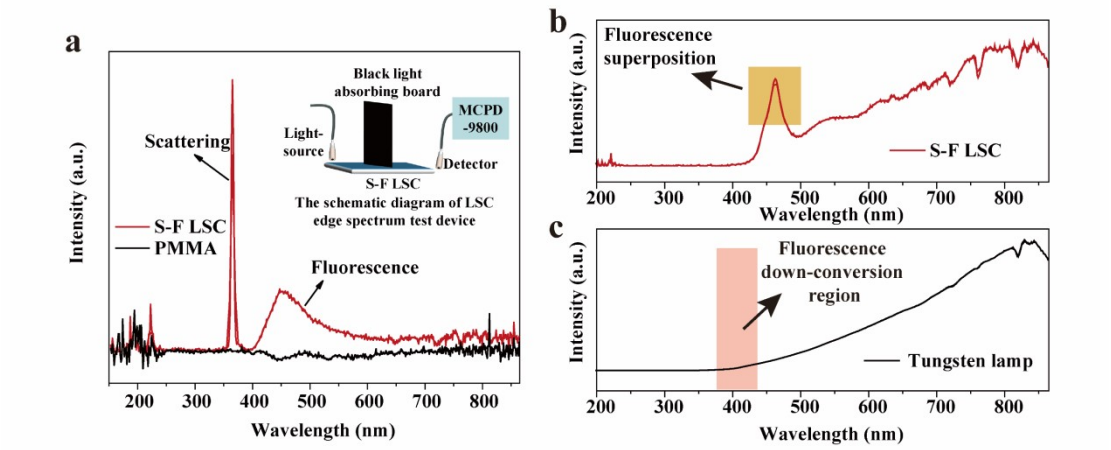


**Fig. S21** LSC edge spectrum under monochromatic light of 365 nm xenon lamp (a). S-F LSC edge spectrum (b) and tungsten lamp light spectrum (c) under tungsten lamp polychromatic light condition.

The specific diagram is shown in the upper right corner of the Fig. S21a. And the spectrum is detected with MCPD-9800. Through this experiment, it is found that the signal of laser scattering to the diagonal edge of S-F LSC at about 365 nm and the signal of fluorescent photons at about 440 nm are simultaneously appeared, which proves the occurrence of scattering and fluorescence, and photons can be transmitted to the edge and emitted from the edge. On the contrary, no characteristic peak was found in pure PMMA under the same conditions (Figure S21a). In addition, a tungsten lamp light source is also used to run the experiment. It is found that a spectrum similar to a tungsten lamp can be detected (see Figure S21b).

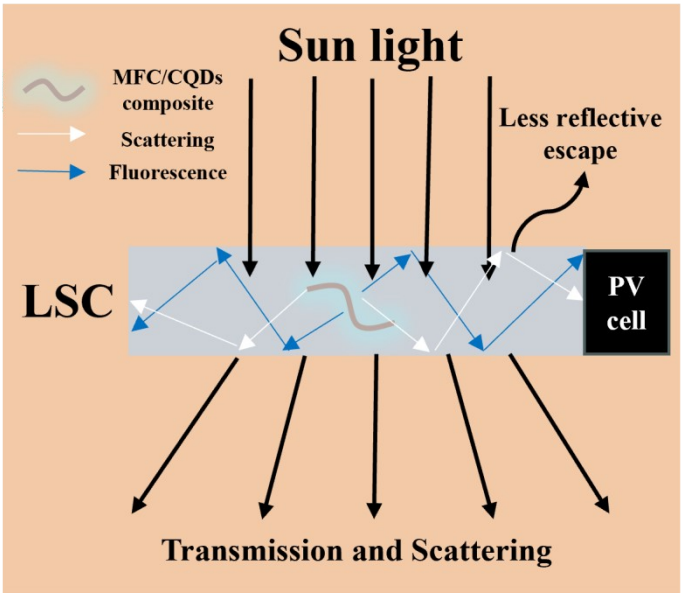


**Fig. S22** The schematic diagram of light propagation in LSC two-dimensional cross section.

The prepared PV-LSC device can effectively capture the light from light scattering and fluorescent luminescence for photoelectric conversion. When the solar light irradiates on the LSC, the MFC/CQDs composites will excite fluorescence and light scattering. Both the fluorescent photons and the scattered photons reach the edge of the LSC through the total reflection in the LSC, which are converted and utilized by the solar cell. In contrast, the functional device prepared by glass or pure PMMA will not guide any photons to the edge.

**Table S1.** Element content of CQDs obtained with different reaction times.

| Samples | C 1s (%) | N 1s (%) | O 1s (%) |
|---|---|---|---|
| CQDs-2H | 62.411 | 7.840 | 29.749 |
| CQDs-2.5H | 65.238 | 5.117 | 29.645 |
| CQDs-3H | 64.699 | 7.025 | 28.276 |
| CQDs-3.5H | 62.498 | 6.612 | 30.890 |
| CQDs-4H | 73.634 | 2.684 | 23.683 |

**Table S2.** Element content of CQDs obtained with different reaction temperatures.

| Samples | C 1s (%) | N 1s (%) | O 1s (%) |
|---|---|---|---|
| CQDs-140 | 66.508 | 5.737 | 27.754 |
| CQDs-150 | 66.108 | 5.922 | 27.970 |
| CQDs-160 | 64.699 | 7.025 | 28.276 |
| CQDs-170 | 66.532 | 6.572 | 26.896 |
| CQDs-180 | 67.884 | 6.142 | 25.975 |

**Table S3.** Relevant parameters of LSCs with different mass fractions of MFC and MFC/CQDs composite.

| Samples | $T_{290\sim390}$ (%) | $T_{390\sim780}$ (%) | $R_{290\sim390}$ (%) | $R_{390\sim780}$ (%) | $A_{290\sim390}$ (%) | $A_{390\sim780}$ (%) |
|---|---|---|---|---|---|---|
| 0 | 79.64 | 92.39 | 7.83 | 7.89 | 12.53 | -0.27 |
| MFC-0.4 | 80.07 | 91.14 | 7.49 | 7.48 | 12.44 | 1.38 |
| MFC-0.8 | 74.41 | 88.07 | 8.20 | 7.85 | 17.39 | 4.07 |
| MFC-1.2 | 70.21 | 86.60 | 9.13 | 8.60 | 20.66 | 4.80 |
| MFC-1.6 | 76.94 | 87.61 | 8.58 | 8.28 | 14.48 | 4.11 |
| MFC/CQDs-0.4 | 67.26 | 87.60 | 7.70 | 8.12 | 25.04 | 4.28 |
| MFC/CQDs-0.8 | 63.16 | 84.68 | 7.74 | 8.25 | 29.10 | 7.06 |
| MFC/CQDs-1.2 | 47.98 | 81.48 | 7.77 | 8.57 | 44.26 | 9.95 |
| MFC/CQDs-1.6 | 46.19 | 77.87 | 8.91 | 9.99 | 44.89 | 12.14 |

T is the transmittance ratio of LSCs at different wavelength ranges of light.

R is the reflection ratio of LSCs at different wavelength ranges of light.

A is the absorption ratio of LSCs at different wavelength ranges of light, which reflects the utilization of visible and ultraviolet light.

A+T+R=100%

**Table S4.** Hazes and PL intensities of LSCs with different mass fractions of MFC and MFC/CQDs composite.

| Samples | Haze (%) | PL intensity (a.u.) |
|---|---|---|
| 0 | 0.19 | 2600 |
| MFC-0.4 | 7.32 | 20680 |
| MFC-0.8 | 29.55 | 15080 |
| MFC-1.2 | 53.50 | 33250 |
| MFC-1.6 | 50.98 | 12140 |
| MFC/CQDs-0.4 | 27.03 | 454930 |
| MFC/CQDs-0.8 | 37.75 | 592010 |
| MFC/CQDs-1.2 | 55.17 | 1042030 |
| MFC/CQDs-1.6 | 69.45 | 1154320 |

**Table S5.** Relevant parameters of LSCs with different concentrations of MFC and MFC/CQDs composite.

| Samples | $J_{sc}$ (mA/cm$^2$) | $V_{oc}$ (V) | *G* | *FF* (%) | $\eta_{opt}$ (%) | *PCE* (%) |
|---|---|---|---|---|---|---|
| Blank (without LSCs) | 1.36 | 0.369 | 2.5 | 55.19 | 3.19 | 0.28 |
| 0 | 10.96 | 0.499 | 2.5 | 65.94 | 7.40 | 3.61 |
| MFC-0.4 | 14.07 | 0.504 | 2.5 | 66.70 | 8.51 | 4.73 |
| MFC-0.8 | 18.86 | 0.515 | 2.5 | 67.78 | 13.49 | 6.58 |
| MFC-1.2 | 21.21 | 0.520 | 2.5 | 68.28 | 13.1 | 7.53 |
| MFC-1.6 | 21.74 | 0.530 | 2.5 | 68.94 | 14.69 | 7.93 |
| MFC/CQDs-0.4 | 19.20 | 0.518 | 2.5 | 67.83 | 10.38 | 6.74 |
| MFC/CQDs-0.8 | 21.29 | 0.523 | 2.5 | 68.31 | 14.14 | 7.60 |
| MFC/CQDs-1.2 | 21.94 | 0.524 | 2.5 | 68.31 | 16.64 | 7.86 |
| MFC/CQDs-1.6 | 23.61 | 0.529 | 2.5 | 68.95 | 18.07 | 8.61 |

**Table S6.** Comparison of different types of PV-LSCs.

| Luminescent substance | Waveguide substrate | Type | Size ($cm^3$) | $\eta_{opt}$ (%) | *PCE* (%) | Transmittance (%) | Ref. |
|---|---|---|---|---|---|---|---|
| MFC-CQDs | PMMA | Intercalation | 2×2×0.2 | 18.07 | 8.61 | 77.81 | This work |
| MFC | PMMA | Intercalation | 2×2×0.2 | 14.69 | 7.93 | 87.6 | This work |
| OSi-CQDs | Glass | Coating | 2.5×2.5×0.1 | 5.89 | 0.148 | 17.86 | [8] |
| Si-CQDs | Glass | Coating | 2.5×2.5×0.1 | 7.58 | 6 | below 20 | [7] |
| Si quantum dots | P(LMA-co-EGDM)/ PLMA | Intercalation | 12×12×0.26 | - | 2.85 | Translucent | [21] |
| Si-CQDs | Glass | Coating | 2.5×2.5×0.1 | 7.1 | - | below 20 | [6] |
| Si-CQDs | Glass | Coating | 5.0×5.0×0.2 | - | 2.09 | 90 | [5] |
| N-CQDs | Glass | Coating | 2.5×1.6×0.1 | 4.75 | 3.94 | above 75 | [9] |
| N-CQDs | PMMA | Intercalation | 2.0×2.0×0.2 | 12.33 | 2.63 | 62 | [17] |
| CQDs | Glass | Coating | 5.0×5.0×0.5 | 4.81 | 2.41 | Transparent | [10] |
| CGAS/ZnS | P(LMA-co-EGDM) | Intercalation | 10×10×0.15 | - | 4.29 | Transparent | [26] |
| $SrAl_2O_4:Eu^{2+}$, $Dy^{3+}$phosphors | Thiol and allyl monomers. | Intercalation | 5.0×5.0×0.5 | 3.38 | 1.37 | below 10% | [24] |
| TPE-MRh | PMMA | Intercalation | 5.0×5.0×0.3 | - | 1.7 | Transparent | [18] |
| SiLRNPs | silicone elastomeric resin | Intercalation | 5.0×5.0×0.6 | 2.12 | - | Transparent | [23] |
| $Mn^{2+}/Yb^{3+}$ codoped $CsPbCl_3$ NCs | PDMS | Intercalation | 13.0×13.0×0.5 | 7.3 | - | 74.2% | [20] |
| $CuInS_2$/ZnS QDs | PMMA | Intercalation | 2.2×2.2×0.3 | 26.5 | 8.71 | Translucent | [19] |
| CdSe-CdS core/shell QDs | Glass | Coating (Sandwich) | 2.8×1.5×0.1 | - | - | Translucent | [15] |
| Donor-emitter fluorophore | PMMA | Coating | 20×20×0.1 | 7.4 | 2.59 | Translucent | [11] |
| PQD | Glass | Coating | 10×10×0.2 | - | 3.3 | 80 | [12] |

**Table S6**. Continued.

| | | | | | | | |
|---|---|---|---|---|---|---|---|
| CdSe@ZnS/ZnS QDs | P(LMA-co-EGDM) | Intercalation | 10×9×0.3 | 7.9 | 2.71 | Translucent | [25] |
| $CuInS_2$ QDs | Glass | Sandwich | 10×10×1 | 8.1 | 2.94 | 43.7 | [16] |
| PbS/CdS core/shell QDs | P(LMA-co-EGDM) | Intercalation | 10×1.5×0.2 | 6.1 | - | Translucent | [27] |
| Perylene bisimide Lumogen F Red 305 (π-Conjugated Polymers) | Glass/ PMMA | Coating | 1.75×1.75×0.15 | 35 (simulation) | - | - | [13] |
| $CuInSexS_2$-x QDs | PLMA | Intercalation | 12×12×0.3 | - | 3.2 | Translucent | [22] |
| 4-(dicyanomethylene)-2-t-butyl-6-(1,1,7,7-tetramethyljulolidyl-9-enyl)-4H-pyran (DCJTB) | Glass | Coating | 25×25×0.2 | - | 5.9 | Translucent | [14] |

"Transparent" defaults that the visible light transmittance exceeds 80 %.

"Translucent" defaults that the visible light transmittance reaches 50-80%.

**References**


1 J. Gan, Q. Lin, Y. Huang, Y. Wu and W. Yu, *ACS Nano*, 2023, **17**, 23512.

2 X. Gong, S. Zheng, X. Zhao and A. Vomiero, *Nano Energy*, 2022, **101**, 107617.

3 W. Kasprzyk, T. Świergosz, S. Bednarz, K. Walas, N. V. Bashmakova, D. Bogdała, *Nanoscale*, 2018, **10**, 13889-13894.

4 W. Kasprzyk, T. Świergosz, P. P. Romańczyk, J. Feldmannc, J, K. Stolarczyk, *Nanoscale*, 2022, 14, 14368-14384.

5 J. Li, J. Chen, X. Zhao, A. Vomiero and X. Gong, *Nano Energy*, 2023, **115**, 108674.

6 Y. Wu, L. Zhao, X. Cao, Y. Zhang, X. Jiang, Z. Sun and Y. Zhan, *Carbon*, 2023, **207**, 77-85.

7 J. Wu, W. Xin, Y. Wu, Y. Zhan, J. Li, J. Wang, S. Huang and X. Wang, *Chem. Eng. J.*, 2021, **422**, 130158.

8 Y. Wu, Y. Zhan, W. Xin, W. Cao, J. Li, M. Chen, X. Jiang, J. Wang and Z. Sun, *ACS. Appl. Energy Mater.*, 2022, **5**, 1781-1792.

9 Y. Li, P. Miao, W. Zhou, X. Gong, X. Zhao, *J. Mater. Chem. A.*, 2017, **5**, 21452-21459.

10 G. Liu, M. Zavelani-Rossi, G. Han, H. Zhao and A. Vomiero, *J. Mater. Chem. A*, 2023, **11**, 8950-8960.

11 B. Zhang, P. Zhao, L. J. Wilson, J. Subbiah, H. Yang, P. Mulvaney, D. J. Jones, K. P. Ghiggino and W. W. H. Wong, *ACS Energy Lett.*, 2019, **4**, 1839-1844.

12 M. Wei, F. P. G. D. Arquer, G. Walters, Z. Yang, L. N. Quan, Y. Kim, R. Sabatini, R. Quintero-Bermudez, L. Gao, J. Z. Fan, F. Fan, A. Gold-Parker, M. F. Toney and E. H. Sargent, *Nat. Energy*, 2019, **4**, 197-205.

13 G. D. Gutierrez, I. Coropceanu, M. G. Bawendi and T. M. Swager, *Adv. Mater.*, 2016, **28**, 497-501.

14 M. J. Currie, J. K. Mapel, T. D. Heidel, S. Goffri and M. A. Baldo, *Science*, 2008, **321**, 226-228.

15 J. Wang, Y. Yuan, H. Zhu, T. Cai, Y. Fang and O. Chen, *Nano Energy*, 2020, **67**, 104217.

16 M. R. Bergren, N. S. Makarov, K. Ramasamy, A. Jackson, R. Guglielmetti and H. McDaniel, *ACS Energy Lett.*, 2018, **3**, 520-525.

17 X. Gong, W. Ma, Y. Li, L. Zhong, W. Li and X. Zhao, *Org. Electron.*, 2018, **63**, 237-243.

18 C. Micheletti, Q. Wang, F. Ventura, M. Turelli, I. Ciofini, C. Adamo and A. Pucci, *Aggregate*, 2023, **3**, e188.

19 C. Li, W. Chen, D. Wu, D. Quan, Z. Zhou, J. Hao, J. Qin, Y. Li, Z. He K. Wang, *Sci. Rep.*, 2016, **5**, 17777.

20 T. Cai, J. Wang, W. Li, K. Hills-Kimball, H. Yang, Y. Nagaoka, Y. Yuan, R. Zia, O. Chen, *Adv. Sci.*, 2020, **7**, 2001317.

21 F. Meinardi, S. Ehrenberg, L. Dhamo, F. Carulli, M. Mauri, F. Bruni, R. Simonutti, U. Kortshagen, S. Brovelli, *Nat. Photon.*, 2017, **11**, 177-185.

22 F. Meinardi, H. McDaniel, F. Carulli, A. Colombo, K. A. Velizhanin, N. S. Makarov, R. Simonutti, V. I. Klimov, S. Brovelli, *Nat. Nanotechnol.*, 2015, **10**, 878-885.

23 F. Corsini, E. Tatsi, A. Colombo, C. Dragonetti, C. Botta, S. Turri, G. Griffini, *Nano Energy*, 2021, **80**, 105551.

24 Y. Zhang, Z. Zheng, X. Cao, G. Gu, Z. Gan, R. Huang, Y. Guo, D. Hou, X. Zhang, *J. Mater. Chem. A*, 2022, **10**, 22145-22154.

25 L. J. Brennan, F. Purcell-Milton, B. McKenna, T. M. Watson, Y. K. Gun'ko, R. C. Evans, *J. Mater. Chem. A*, 2018, **6**, 2671-2680.

26 Y. You, X. Tong, A. I. Channa, H. Zhi, M Cai, H. Zhao, L. Xia, G. Liu, H. Zhao, Z. Wang, *Chem. Eng. J.*, 2023, **452**, 130490.

27 Y. Zhou, D. Benetti, Z. Fan, H. Zhao, D. Ma, A. O. Govorov, A. Vomiero, F. Rosei, *Adv. Energy Mater.*, 2016, **6**, 1501913.